

New Approaches to In Situ Calibration for Seafloor Geodetic Measurements

William S. D. Wilcock
School of Oceanography
University of Washington
Seattle, U.S.A.
wilcock@uw.edu

Dana A. Manalang
Applied Physics Laboratory
University of Washington
Seattle, U.S.A.
manalang@uw.edu

Michael J. Harrington
Applied Physics Laboratory
University of Washington
Seattle, U.S.A.
mikeh@apl.washington.edu

Erik K. Fredrickson
School of Oceanography
University of Washington
Seattle, U.S.A.
erikfred@uw.edu

Geoff Cram
Applied Physics Laboratory
University of Washington
Seattle, U.S.A.
cramg@apl.washington.edu

James Tilley
Applied Physics Laboratory
University of Washington
Seattle, U.S.A.
jtilley@apl.washington.edu

Justin Burnett
Applied Physics Laboratory
University of Washington
Seattle, U.S.A.
jburnett@apl.washington.edu

Derek Martin
Applied Physics Laboratory
University of Washington
Seattle, U.S.A.
dtmartin@apl.washington.edu

Taro Kobayashi
Paroscientific, Inc.
Redmond, WA
taro@paroscientific.com

Jerome M. Paros
Paroscientific, Inc.
Redmond, WA
paros@paroscientific.com

Abstract—Seafloor geodesy is challenging but important for understanding the hazards from earthquakes and tsunamis along subduction zones. Two methods of seafloor geodesy are presented based on obtaining self-calibrated measurements with resonant quartz crystal technology sensors. The A-0-A method for calibrating pressure observations utilizes the internal pressure of the instrument housing as a reference pressure to calibrate sensor drift. An 8-month seafloor test at a depth of 900 m, shows the method has reduced the relative drift between two pressure sensors to <1 mm. The rotating (or flipping) tiltmeter calibrates the accelerations of the horizontal channels of a tri-axial accelerometer by rotating them into the vertical where the acceleration of gravity is used as a reference acceleration. Laboratory tests are very promising and deployments are planned on the seafloor and at a geodetic observatory.

Keywords— seafloor geodesy, pressure, tiltmeter, subduction zone hazards

I. INTRODUCTION

In continental settings, geodetic observations from dense networks of Global Positioning System stations and maps of ground displacement obtained using interferometric synthetic aperture radar have revolutionized our ability to understand tectonic and volcanic processes [1]. Because the oceans do not transmit the electromagnetic waves that enable these techniques, geodetic measurements on the seafloor are much more challenging but they are nevertheless very important. Subduction zones host the largest and some of the most destructive earthquakes, and the seismogenic zones that slip during large earthquakes generally lie primarily offshore. To characterize and mitigate the seismic and tsunamigenic risk, seafloor geodesy is essential to determine where megathrust

faults are locked and where they are partially or completely slipping by steady creep or episodic slow slip. Seafloor geodesy is also necessary for monitoring the stability of underwater slopes and for improving our scientific understanding of dynamic processes at ocean spreading centers, transform faults, and hotspot volcanoes.

There are a variety of approaches to seafloor geodesy [2], [3] and in general, different techniques are complementary, either because they measure different components of displacement and strain, or because redundant measurements provide a check on reliability that would otherwise be difficult to obtain. In this paper, we describe two methods of seafloor geodesy that employ resonant quartz crystal technology to obtain self-calibrated geodetic measurements. First, the A-0-A approach to calibrated pressure measurements utilizes the internal pressure of the pressure housing as a reference pressure to determine sensor drift. We report on the first non-proprietary ocean test of this approach. Second, the rotating (or flipping) tiltmeter calibrates the drift on the two horizontal channels of a three-component accelerometer by periodically rotating each one into a vertical orientation where the acceleration of gravity is used as a reference. This approach has been tested in the laboratory and tests on the seafloor and at a geodetic observatory on land will commence soon.

II. VERTICAL GEODESY

Time series observations of seafloor pressure are of value for both geophysical and oceanographic studies because they are sensitive to the combined effects of changes in the elevation of the seafloor and changes in the vertically integrated weight of the overlying water column and

Support for the SCTA development from National Science Foundation award 1634103 and the University of Washington Royalty Research Fund.

atmosphere. However, conventional pressure measurements are limited for many applications, because the most widely used and highest resolution pressure sensors, manufactured by Paroscientific Inc., are subject to long-term drift at a typical rate of ~ 1 part in 10^4 per year, which cannot be predicted from laboratory calibrations before and after a seafloor deployment [4]–[6]. For geodetic applications, bottom pressure time series have been used successfully in subduction zones to detect offshore slow-slip earthquakes lasting a few weeks [7], [8]. However, the drift rates are too large to measure the long-term rates of steady secular strain from plate tectonic motions above a locked fault, and so in-situ calibration is important.

A. Approach

One approach to eliminating sensor drift from measurements of secular strain is to conduct closed loop surveys with a mobile pressure recorder (MPR) [9], [10]. An MPR is transported over several passes around a network of benchmarks by a remotely operated vehicle (ROV). Repeat visits to each benchmark are used to solve for the drift of the MPR after first correcting for tides and thus, measure the relative elevations of the benchmarks. This method is inherently expensive because it requires long dives with an ROV and is limited in scale to networks spanning ~ 10 km because of the transit speeds of ROVs.

Another approach is to incorporate a means of calibration into a bottom pressure recorder, itself. The Self Calibrating Pressure Recorder (SCPR) [11], [12] employs a redundant pair of Paroscientific quartz pressure gauges that record ambient seawater pressure continuously, except for periodic short calibration intervals when they are connected by a valve to a dead-weight tester, a device that combines an accurately measured mass and a rotating oil-filled piston cylinder to generate a known pressure that is accurate to ~ 1 cm of water. For each SCPR deployment, the mass in the dead-weight tester is changed so that the pressure closely matches that to be observed on the seafloor. Both the MPR and SCPR approaches have been used successfully to resolve the uplift of Axial Volcano in the Northeast Pacific Ocean with an uncertainty of ~ 1 cm/yr [11], [13].

The A-0-A approach to calibration is similar conceptually to the SCPR, except that the deadweight tester is replaced by the internal pressure of the sensor housing measured by an accurate barometer, leading to an instrument that is more compact and less complex. The method relies on the assumption that the span of the sensor remains constant, that is the drift rate at low pressures and high pressures is the same. Laboratory measurements at the Japanese National Institute of Advanced Industrial Science and Technology (AIST) support this assumption [14], but seafloor tests are important to demonstrate the methods.

The University of Washington Geodetic and Seismic Sensor Module (GSSM) (Figs. 1, 2a) packages a Paroscientific Seismic + Oceanic Sensors (SOS) unit for deployment at 900 m depth on the Monterey Advanced Research System (MARS) cabled observatory in Monterey Bay. The SOS unit comprises two Paroscientific absolute pressure gauges which for this deployment have a maximum depth rating of 1400 m, an accurate Paroscientific barometer measuring the internal pressure of the pressure case, a Quartz Seismic Sensors tri-axial accelerometer, and Paroscientific nano-resolution processing electronics. In the GSSM, the oil filled lines to the pressure sensors are connected to a 3-way Swagelok ball valve that is operated by a Hanbay motorized actuator to switch between external and internal pressure for calibrations. Because a small amount of oil leaks through the valve each time it turns, there are external and internal oil reservoirs. The internal fluid reservoir for this deployment was a simple cup, open at the top with a wide cross-sectional area to minimize the changes in pressure head through the deployment. The external oil reservoir is designed for ~ 200 valve cycles. The MARS cabled observatory provides power, communications to retrieve data and control the valve, and precise one pulse per second timing. Custom electronics condition the incoming observatory power and custom software provides a user interface through which operators can control the internal valve and sensors in real time from shore.

B. Results

The GSSM was deployed in June 2017 (Fig. 2b) and has been configured to stream serial data from the sensors to a

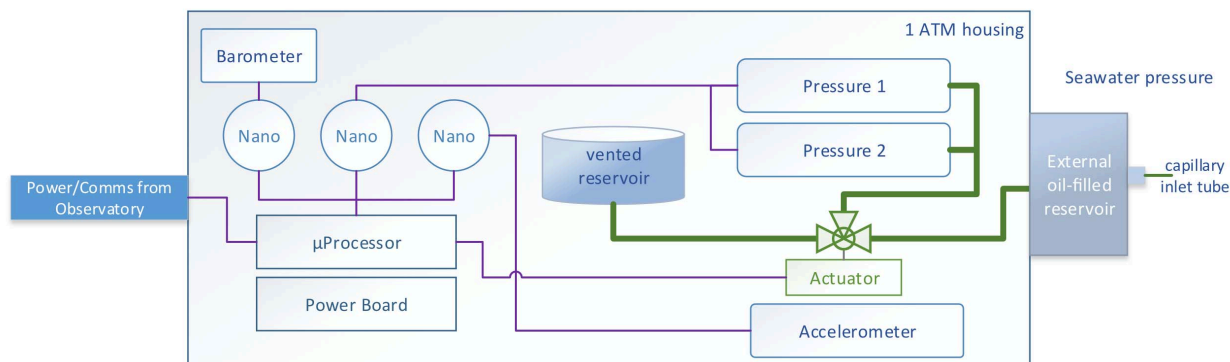


Fig. 1. GSSM block diagram. A pair of pressure sensors connect to an actuator-controlled, 3-way ball valve that toggles between external seawater pressure and internal housing pressure of 1 atmosphere by sending commands from shore. The barometer provides an accurate reference measurement of internal housing pressure. An accelerometer continuously monitors seafloor motion. Three Paroscientific Nano-Resolution Electronics boards capture high resolution sensor measurements, timestamping them and passing them in real time to on-shore computers through the microprocessor. Thick green lines represent oil-filled plumbing. Thin purple lines represent data paths.

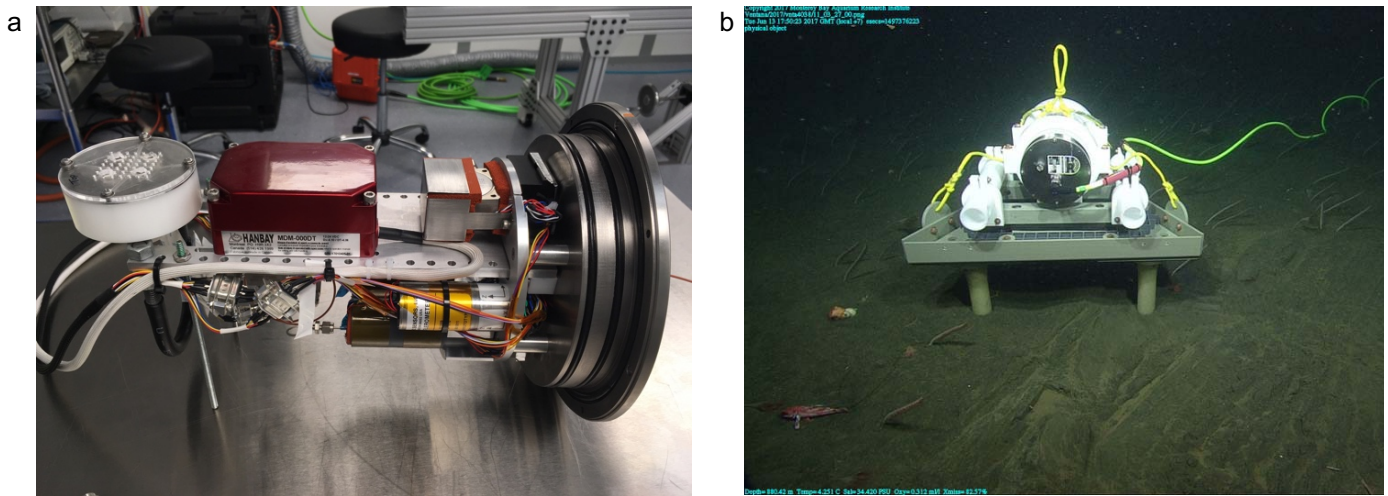


Fig. 2. The Geodetic and Seismic Sensor Module (a) in the laboratory and (b) on the seafloor attached to the MARS cabled observatory.

laptop in the shore station at a sample rate of 40 Hz for the pressure sensors and accelerometer, and at 1 Hz for the barometer. As of early March, 2018, a total of 87 five-minute calibrations have been performed at an interval that was initially once per day but has now decreased to once per week.

Fig. 3 shows an example of 1 day of data that includes a calibration. The two redundant pressure sensors in the GSSM track the external pressure with an offset of ~ 2 cm of water and the high frequency sampling rates on the GSSM allow the pressure sensor to record infragravity waves and microseisms (Fig. 3, inset) as well as earthquakes.

Fig. 4 shows the pressures recorded during a calibration. It takes a few seconds to turn the valve from external to internal pressure which leads to a sudden drop in pressure. The measured pressures overshoots (Fig 4., inset), because the

adiabatic expansion of the oil leads to cooling and it takes some time for thermal equilibrium to be achieved, and because of short term viscoelastic transients. During the calibration, the pressures recover approximately exponentially and we chose to measure the calibration pressure by averaging pressures from 3 minutes to 4 minutes after the onset of the calibration (Fig. 4). The pressures on the two pressure sensors are compared to the accurate barometer to get the offset of each pressure sensor from the true pressure.

Fig. 5a shows the offsets from the barometer (subtractive pressure corrections) for both pressure sensors for all the calibrations. Early on in the GSSM operation, the valve actuator was turned on prior to each test, but after two weeks (10 tests), we decided to leave the actuator permanently on. As a result, the temperature inside the housing rose 1°C from

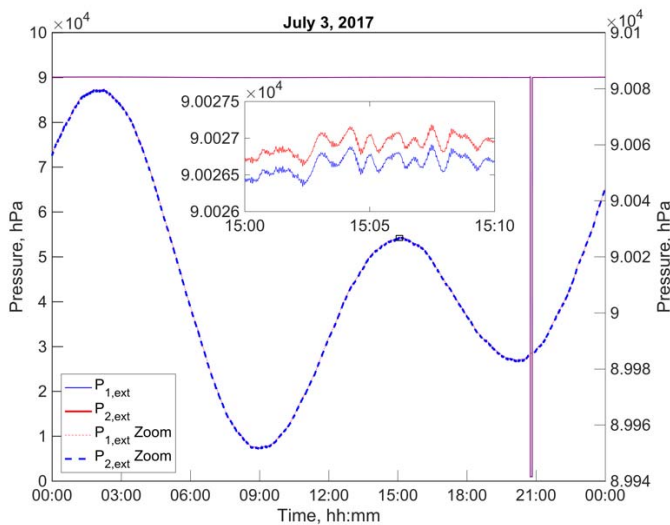


Fig. 3. Example of one day of pressure data from the GSSM showing pressures at full scale with an A-0-A test visible just before 21:00 and on a scale which shows the tides. The inset figure, of 10 minutes of data shows that the high-resolution pressure data detects infragravity waves with periods of ~ 1 minute and smaller amplitude microseisms with periods of a few seconds. Note that 1 hPa is equivalent to 1 cm of water.

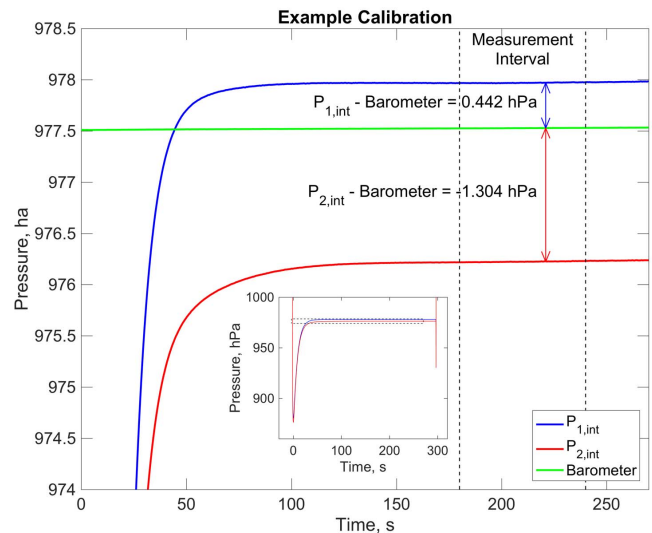


Fig. 4. Pressures measured by the GSSM for the two pressure sensors and the barometer for an example calibration measurement. The average pressure recorded from 180 s to 240 s into the test on the two pressure sensors is compared to the barometer to obtain a low pressure offset between the pressure sensors and the true pressure.

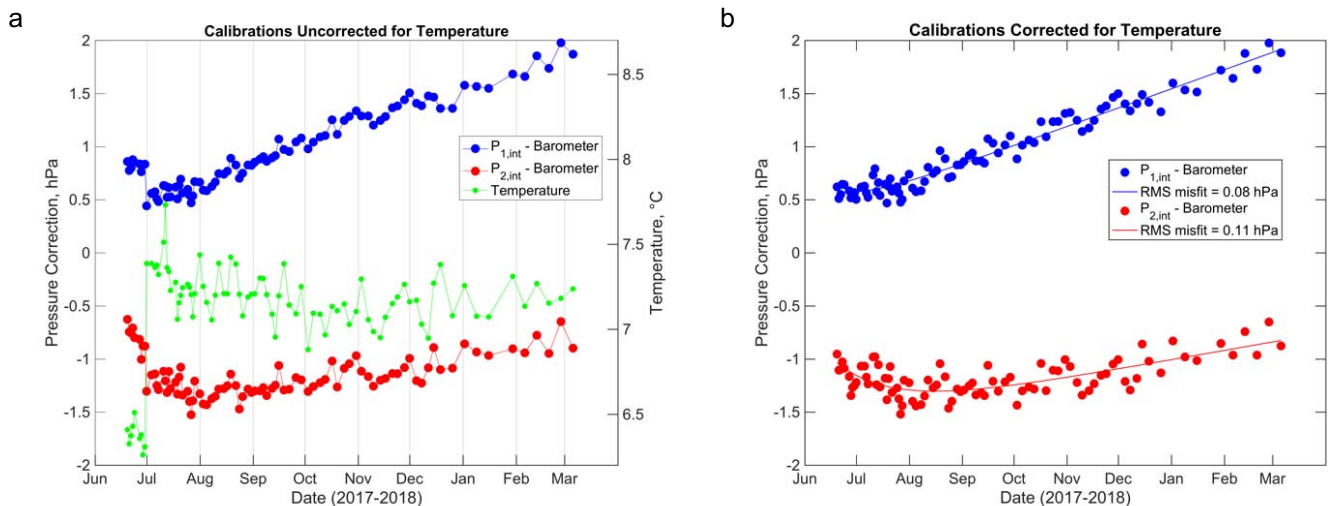


Fig. 5. (a) Calibration pressure corrections (pressure sensor minus barometer) for the two pressure sensors and the temperature for the A-0-A calibrations. (b) Calibration pressure corrections, corrected for temperature and fit with an exponential + linear drift curve.

~6.4°C to ~7.4°C. There is a noticeable jump in the offsets associated with the increase in temperature which indicates that the thermal terms in the calibration coefficients provided by Paroscientific have small inconsistencies (the factory temperature calibrations are determined for a wide temperature range and are not as accurate as could be obtained by calibrating the sensors over a narrow temperature range). Aside from this temperature-related jump the calibration measurements show a relatively smooth progression with each sensor drifting to higher pressures by the end of the period of observation.

To characterize the drift of each sensor we used a least squares method to fit the calibration offsets for each sensor with a function of the form:

$$p(t) = a \exp(-bt) + ct + d + e(T - T_{ref}) \quad (1)$$

where $p(t)$ is the pressure offset as a function of the time since deployment, t ; T is temperature with a reference temperature, T_{ref} , set to the median temperature of the tests; and a , b , c , d , and e are constants. The exponential and linear terms are commonly used to model the drift of Paroscientific pressure sensors [5], [6]. The resulting calibration curves with the temperature correction applied to the data are shown in Fig. 5b. The calibration curves fit the offsets on each sensor with an RMS misfit of ~0.1 hPa (1 mm of water).

We cannot directly test the assumption that the span of the pressure sensors is invariant, but because there are redundant pressure sensors in the GSSM, we can test the consistency of the spans throughout the deployment by calculating the differences between the external pressures measured just before each calibration and the internal pressure measured during the calibration, and comparing these differences for the two sensors. After solving to remove a linear temperature correction, the difference in the spans (Fig. 6a) has remained consistent to ~0.07 hPa and since the start of November and appears to be changing at a rate of ~0.15 hPa per year (1.5 mm of water per year). Fig. 6b compares the uncorrected and corrected relative drift of the two sensors.

The simplest explanation of the test is that spans of the two sensors remain constant to <1 mm over the 8 months of the test to date and that the smooth curves that fit the calibration data can correct the pressure records to a precision of ~1 mm over 8 months. This is about a two order of magnitude reduction in the drift seen in some uncalibrated pressure sensors [5]. The drift of the frequency-counting clocks used to measure the frequency output of the pressure sensors will contribute sensor drift that is common to both sensors. For cabled installations, this could be corrected by calibrating the counting clocks using the timing signals provided by the observatory, although this is not being done for this deployment.

III. TILT MEASUREMENTS

Measurements of horizontal tilt are another geodetic observation that can be made both on land and underwater. There are two basic approaches to measuring geological tilt; short-baseline measurements seek to observe directly the change in attitude of a platform coupled to the ground and long-baseline measurements obtain tilt based on the relative change in elevation between two sites [15], [16]. Many modern short-baseline tiltmeters use electrodes to sense the position of an air bubble in a curved tube filled with an electrolytic solution. Other approaches include using optical techniques to measure the deflection of a pendulum and measuring the changes in the electrical field needed to hold a magnetized pendulum in place [17]. A typical bubble level tiltmeter will drift at a rate of $\gg 10 \mu\text{rad}/\text{yr}$. There is a tradeoff between precision and dynamic range so that in rapidly deforming settings, the most precise short-baseline measurements often require that the instrument be re-leveled when it moves off scale. Long baseline tiltmeters generally use optical or electromagnetic methods to measure the relative change in water level between the ends of a long, buried pipe (typically 100 m to 1 km long). They can provide precise and stable measurements but are expensive to install and have not been developed for the seafloor.

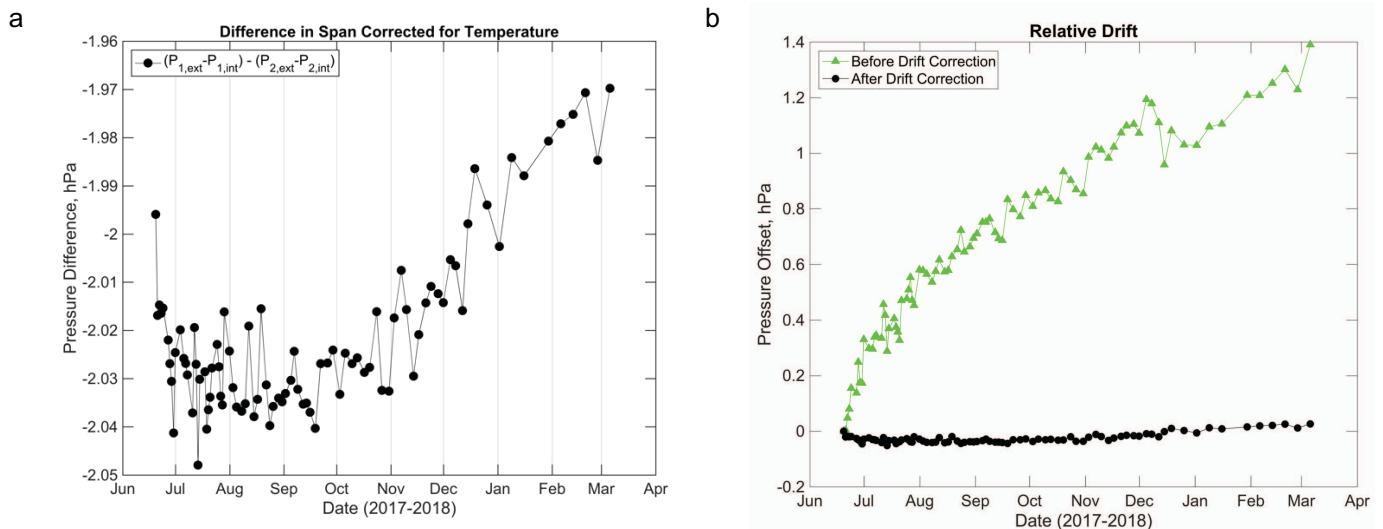


Fig. 6. (a) Differences in span of the two pressure sensors corrected for temperature. (b) Relative drift of the two sensors before and using the calibrations to correct for drift.

A common problem with using short-baseline tiltmeters on land is that it can be difficult to separate signals related to tectonic deformation from changes in tilt related to soil expansion, groundwater variations and snow loads [16]. In the oceans, sources of noise include bottom currents, tides and ocean weather systems. On active volcanoes, the signals associated with magmatic inflation and deflation and shorter-term events can exceed local effects and for this reason short-baseline tiltmeters are widely used by volcanologists [18]. Elsewhere where the expected signals are smaller, it is common to deploy tilt meters in deep boreholes in order to get below surficial effects and ensure good coupling to the ground. In such settings the stability and noise levels (repeatability) of the tiltmeter are particularly important considerations.

A. Approach

The tiltmeter we are developing is based on a tri-axial quartz crystal accelerometer developed by Quartz Seismic Sensors Inc. [19]. The accelerometer has a full-scale deflection of $\pm 3g$ and is capable of very precise measurements with a resolution of a few parts per billion when samples are averaged over 1 second. The factory calibration involves determining an alignment matrix which mathematically corrects the three components so that they are orthogonal and is used to calculate the total scalar acceleration which is independent of orientation. If the accelerometer is oriented so one channel is vertical, the vertical channel measures an acceleration of 1 g and the two horizontal channels measure ~ 0 g. Changes in the tilt, ϕ , of a horizontal channel will lead to a signal of $g \sin \phi \approx g\phi$ so the accelerometer can be used as a tiltmeter. However, as is the case for pressure observations, without calibration, sensor drift limits the long-term measurement of secular strain. The approach to correcting the horizontal channels for sensor drift is to conduct a periodic calibration by rotating (or flipping) each horizontal channel into the vertical for a short interval to measure Earth's gravity vector, g [20]. Since g is to a high degree of accuracy invariant at any location, changes in the measurement of g between successive rotations can be

attributed to sensor drift. This measurement of drift can then be used to correct each horizontal accelerometer channel to obtain a time series of true tilt changes between calibrations.

The University of Washington Self-Calibrating Tilt Accelerometer (SCTA) (Figs. 7, 8) employs a gimbal mechanism in which the accelerometer is rotated about two orthogonal axes using Lin Engineering stepper motors that can be locked in position by electromagnetic brakes from Stock Drive Products. Each motor is fitted with a US Digital incremental encoder. When operated in microstepping mode, each motor-encoder pair can repeatably position its gimbal axis very precisely for calibration and back to tilt-measurement mode. In order to minimize thermal transients (which can affect accelerometer outputs) within the housing, the motors are powered off when in tilt-measurement mode. The brakes have been specified to be power-off to engage, which means that they also contribute minimally to thermal transients when they lock each axis during tilt measurement.

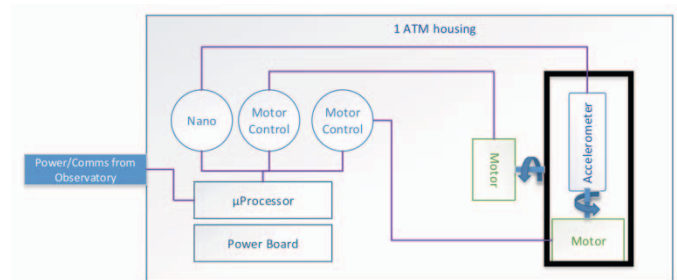


Fig. 7. SCTA block diagram. A tri-axial quartz crystal accelerometer can be rotated in a tow axis gimbal driven by two stepper motors. The accelerometer continuously monitors seafloor motion and tilt. The drift in the accelerometer bias can be measured by periodically rotating the two horizontal channels to measure the Earth's gravity vector. One Paroscientific Nano-Resolution board captures high-resolution sensor measurements at 40 Hz, timestamping them and passing them in real time to onshore computers through the microprocessor.

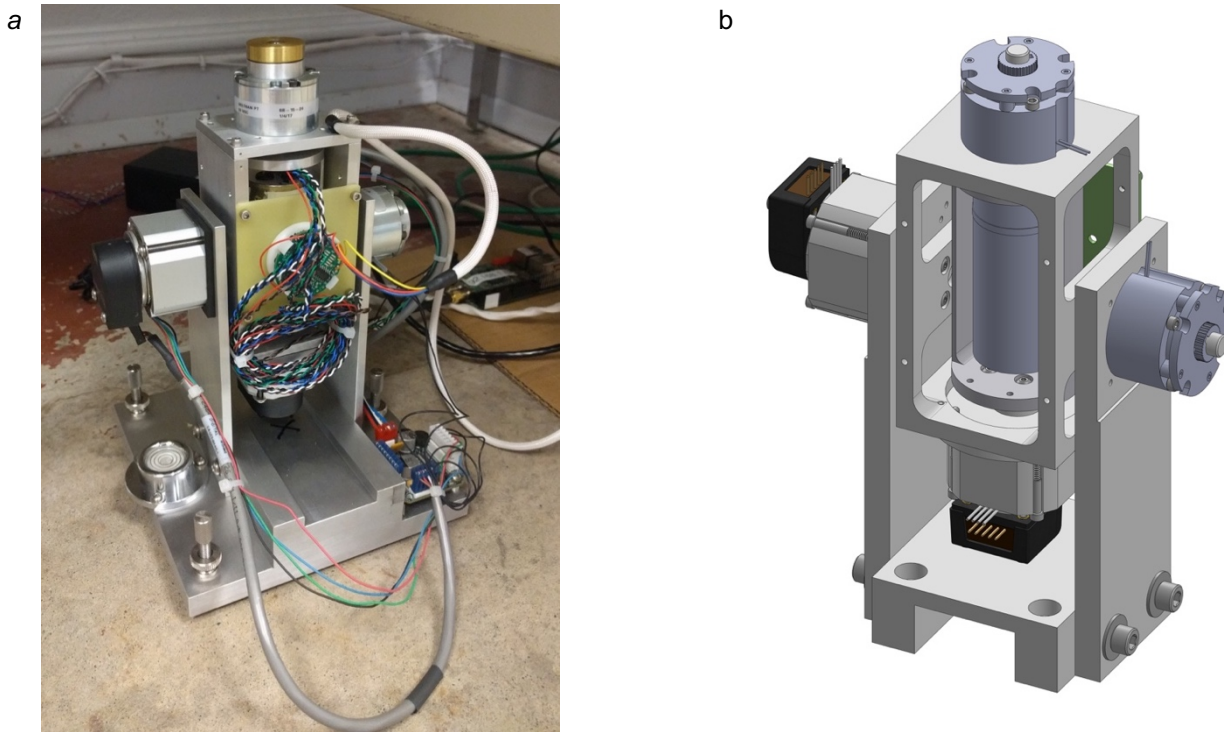


Fig. 8. (left) Photograph of laboratory prototype of the Self-Calibrating Tri-axial Accelerometer (SCTA) tiltmeter comprising a tri-axial accelerometer that is rotated about two axes with stepper motors and held in position by electromagnetic brakes. (right) Three-dimensional rendering of the SCTA being built for testing on the seafloor and at a geodetic observatory.

B. Testing

We have undertaken quite extensive testing of the calibration approach, first flipping the accelerometer by hand and then with the prototype SCTA apparatus (Fig 8a). We have explored a number of different rotation sequences for the calibration measurements but our preferred choice for the initial deployments is as follows: The outer gimbal is first

rotated by 90° to place the long (Z-channel) axis of the accelerometer horizontal with the Z-channel vertical and locked for a two-minute calibration measurement. The inner gimbal is then rotated 90° so that the Y-channel is vertical and locked for a two-minute calibration measurement. The inner gimbal is then rotated back so that the X-channel is again vertical and locked for a second two-minute calibration. Finally, the outer gimbal is rotated back so that the Z-channel is again vertical and locked in the standard orientation for observations. Fig 9. shows the accelerations measured during an example calibration.

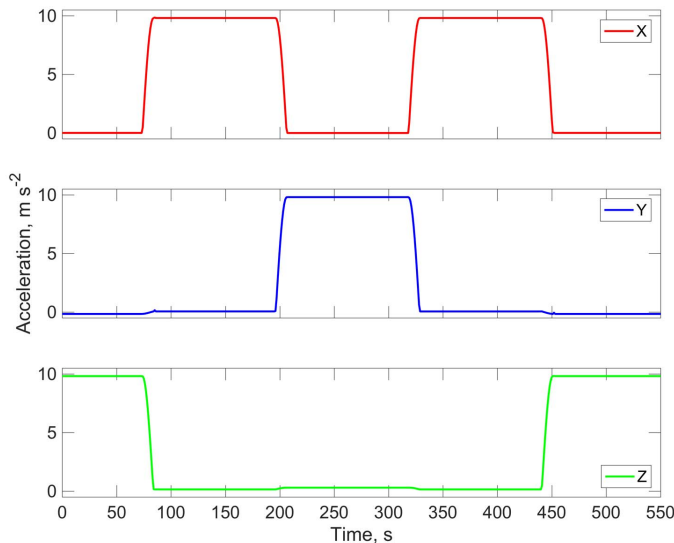


Fig. 9. Accelerations recorded on the three accelerometer channels during a calibration

Fig. 10 shows the calibration measurements obtained during a 52-day laboratory test in December 2017 and January 2018. Calibration were performed daily for the first 11 days and then weekly for the remainder of the test. The three sets of calibration measurements (1st X, Y and 2nd X) show smooth increases in the measured g of $\sim 10^{-4} \text{ m s}^{-2}$ over the duration of the vertical with an accuracy of better than 1° . Since the total acceleration is dominated by the channel that is nearly vertical ($\cos(1^\circ) = 0.9998$), the drift of the measured total acceleration is to a high degree of accuracy that of the channel that is vertical. The average drift rates determined were $6.63 \times 10^{-4} \text{ m s}^{-2} \text{ yr}^{-1}$ and $9.76 \times 10^{-4} \text{ m s}^{-2} \text{ yr}^{-1}$ for the X and Y channels, respectively. The drift rates are somewhat smaller than those determined by factory calibrations in March 2017 and February 2018 that are spaced 318 days apart (Table 1), consistent with an expected decrease in drift rate as the sensor ages.

There is an offset between the first and second X calibration which is a result of the fact that there are short term transient responses induced by re-orienting the accelerometer

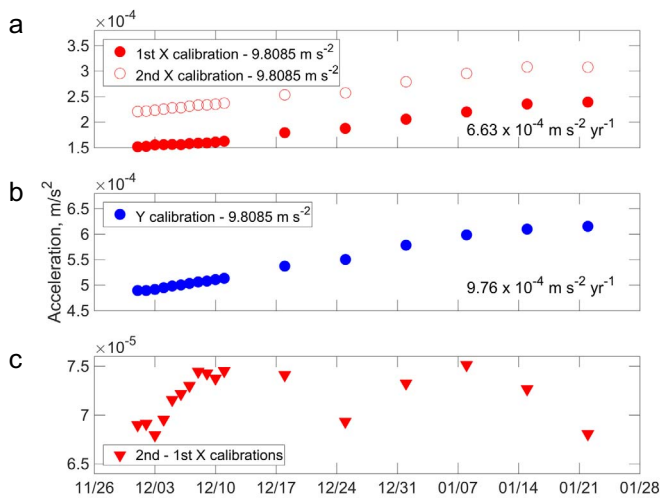


Fig. 10. Calibration measurements for a 52-day laboratory test. (a) Total acceleration measured when the X-channel is vertical. There are two measurements for each calibration). The inferred drift rate is $6.63 \times 10^{-4} \text{ m/s}^2 \text{ yr}^{-1}$. (b) Total acceleration measured when the Y-channel is vertical. The inferred drift rate is $9.76 \times 10^{-4} \text{ m/s}^2 \text{ yr}^{-1}$. (c) The difference of the two acceleration measurements when the X-channel is vertical.

so that the second X calibration is influenced by the two calibrations that came before it. The difference between the 1st and second X calibration (Fig. 10c) is consistent to 10^{-5} m/s^2 over the testing period, which shows that these transient terms are quite predictable and provides an indication of the reliability of each calibration. It also illustrates the importance of performing calibrations with a consistent sequence of timed rotations. The offset of successive calibration measurements can be used to determine the drift of each channel during an observation interval and thus, to apply a linear correction to the tilts measured by the X and Y channels. There is no need to return the X and Y channels to the exact same orientations after a calibration because the accumulated tilt is determined independently for each time segment between calibrations.

TABLE I. AVERAGE DRIFT RATES OF THE ACCELEROMETER DETERMINED OVER 318 DAYS FROM FACTORY CALIBRATIONS

S/N	Axis	Offset, m/s^2		Drift Rate, $\text{m/s}^2 \text{ yr}^{-1}$
		Mar 28, 2017	Feb 9, 2018	
501021	X	-0.128×10^{-3}	1.00×10^{-3}	1.29×10^{-3}
501022	Y	0.098×10^{-3}	1.42×10^{-3}	1.52×10^{-3}
501023	Z	0.086×10^{-3}	1.12×10^{-3}	1.19×10^{-3}

In the laboratory, the tilt signals are large and unknown and therefore we have no means of determining how well the drift-corrected measurements represent the true history of tilt. For this reason, we are planning two field tests. First, an SCTA will be deployed on the Ocean Observatories Initiative Cabled Array in the center of Axial Seamount next to a bottom pressure and tilt instrument that incorporates a Jewell Instruments high-resolution LILY tiltmeter. This will allow a direct comparison between the SCTA and the LILY tiltmeter in a setting where the signals are quite large (Axial Seamount is presently inflating at $\sim 40 \text{ cm/yr}$). Second, an SCTA will be

deployed on the floor of a buried vault in the Scripps Institution of Oceanography Cecil and Ida Green Piñon Flat Observatory (PFO) where the output can be compared to long-baseline tilt measurements [15]. Ultimately, the SCTA will require testing in a quiet borehole setting

ACKNOWLEDGMENT

We thank the engineers at Paroscientific, Inc. for guidance and support during the development of the GSSM and SCTA. The MARS team at the Monterey Bay Aquarium Research Institute have provided engineering support throughout the design, testing, deployment and operations of the GSSM.

REFERENCES

- [1] R. Bürgmann and W. Thatcher, "Space geodesy: A revolution in crustal deformation measurements of tectonic processes," *Special Paper of the Geol. Soc. Am.*, vol. 500, pp. 397–430, 2013.
- [2] R. Bürgmann and D. Chadwell, "Seafloor Geodesy," *Ann. Rev. Earth Planet. Sci.*, vol. 42, no. 1, pp. 509–534, 2014.
- [3] H. Fujimoto, "Seafloor geodetic approaches to subduction zone thrust earthquakes," *Monogr. Environ. Earth Planets*, vol. 2, pp. 23–63, 2014.
- [4] H. Matsumoto, E. Araki, K. Kawaguchi, S. Nishida, and Y. Kaneda, "Long-term features of quartz pressure gauges inferred from experimental and in-situ observations," in *OCEANS 2014 - TAIPEI*, 2014, pp. 1–4.
- [5] A. Polster, M. Fabian, and H. Villinger, "Effective resolution and drift of Paroscientific pressure sensors derived from long-term seafloor measurements," *Geochem. Geophys. Geosyst.*, vol. 10, no. 8, p. Q08008, Aug. 2009.
- [6] D. R. Watts and H. Kontoyiannis, "Deep-Ocean Bottom Pressure Measurement: Drift Removal and Performance," *J. Atmos. Oceanic Technol.*, vol. 7, no. 2, pp. 296–306, Apr. 1990.
- [7] L. M. Wallace *et al.*, "Slow slip near the trench at the Hikurangi subduction zone, New Zealand," *Science*, vol. 352, no. 6286, pp. 701–704, May 2016.
- [8] Y. Ito *et al.*, "Episodic slow slip events in the Japan subduction zone before the 2011 Tohoku-Oki earthquake," *Tectonophysics*, vol. 600, pp. 14–26, Jul. 2013.
- [9] W. W. Chadwick, Jr., S. L. Nooner, M. A. Zumberge, R. W. Embley, and C. G. Fox, "Vertical deformation monitoring at Axial Seamount since its 1998 eruption using deep-sea pressure sensors," *J. Volcanol. Geotherm. Res.*, vol. 150, no. 1, pp. 313–327, 2006.
- [10] S. L. Nooner, S. C. Webb, W. R. Buck, and M.-H. Cormier, "Post Eruption inflation of the East Pacific Rise at $9^{\circ}50' \text{ N}$," *Geochem. Geophys. Geosyst.*, vol. 15, no. 6, pp. 2676–2688, Jun. 2014.
- [11] G. Sasagawa, M. J. Cook, and M. A. Zumberge, "Drift-corrected seafloor pressure observations of vertical deformation at Axial Seamount 2013–2014," *Earth Space Sci.*, vol. 3, no. 9, p. 2016EA000190, Sep. 2016.
- [12] G. Sasagawa and M. A. Zumberge, "A Self-Calibrating Pressure Recorder for Detecting Seafloor Height Change," *IEEE J. Oceanic Eng.*, vol. 38, no. 3, pp. 447–454, Jul. 2013.
- [13] S. L. Nooner and W. W. Chadwick Jr., "Volcanic inflation measured in the caldera of Axial Seamount: Implications for magma supply and future eruptions," *Geochem., Geophys., Geosyst.*, vol. 10, no. 2, p. Q02002, 2009.
- [14] H. Kajikawa and T. Kobata, "Reproducibility of calibration results by 0-A-0 pressurization procedures for hydraulic pressure transducers," *Meas. Sci. Technol.*, vol. 25, no. 1, p. 015008, 2014.
- [15] D. C. Agnew, "Before PBO: An Overview of Continuous Strain and Tilt Measurements in the United States," *J. Geodetic Soc. Japan*, vol. 53, no. 2, pp. 157–182, Jun. 2007.
- [16] D. C. Agnew, "Strainmeters and tiltmeters," *Rev. Geophys.*, vol. 24, no. 3, pp. 579–624, 1986.

- [17] M. Hensch, "On the interrelation of fluid-induced seismicity and crustal deformation at the Columbo Submarine Volcano (Aegean Sea, Greece)," Ph.D., University of Hamburg, 2009.
- [18] D. Dzurisin, "A comprehensive approach to monitoring volcano deformation as a window on the eruption cycle," *Rev. Geophys.*, vol. 41, no. 1, Feb. 2003.
- [19] Paroscientific, Inc., "Triaxial accelerometers for improved seismic and geodetic measurements", Technical Note, Doc No G8096 Rev. D., http://www.paroscientific.com/pdf/G8096_Triaxial_Accelerometer.pdf
- [20] J. M. Paros, "Triaxial accelerometer assembly and in-situ calibration method for improved geodetic and seismic measurements," US Patent 9,645,267, 2017.